Subwavelength imaging with a fishnet flat lens

Zeyong Wei,[1,2] Yang Cao,[3] Zhijie Gong,[1,2] Xiaopeng Su,[1,2] Yuancheng Fan,[1,2] Chao Wu,[1,2]
Junwu Zhang,[4] and Hongqiang Li[1,2,*]

[1]*MOE Key Laboratory of Advanced Micro-Structured Materials, Shanghai 200092, China*
[2]*School of Physics Science and Engineering, Tongji University, Shanghai 200092, China*
[3]*Shanghai Radio Equipment Institute, Shanghai 200090, China*
[4]*Beijing Institute of Space Long March Vehicle, Beijing 100076, China*

(Received 9 August 2013; published 13 November 2013)

We theoretically and experimentally investigate subwavelength imaging with a flat lens constructed with fishnet metamaterial. By adopting a ring antenna with a diameter of 5 mm, a high-quality image, with the full width at half maximum no more than half of the operational wavelength at 10 GHz, is measured in free space at a distance of 19 mm away from the flat lens. The spatial resolution is about one third of the operational wavelength considering the electrical size of the ring antenna, which is also verified by finite-difference time-domain simulations. The subwavelength imaging arises from the negative coupling between the adjacent spoof plasmonic waveguides of fishnet metamaterial and is proved valid in a wide frequency range.

DOI: 10.1103/PhysRevB.88.195123 PACS number(s): 78.67.Pt, 42.70.Qs, 44.40.+a, 42.70.Km

I. INTRODUCTION

Conventional imaging systems suffer from the diffraction limit for their spatial resolution. This is because the spatial details of an object, which are finer than operational wavelength λ in scale, are carried by evanescent waves and thus cannot propagate in the far field.[1] Substantial efforts have been devoted to overcoming the diffraction limit in different ways, such as using the superoscillation of helical waves,[2] resorting to a higher order of harmonic generations,[3] etc.[4,5] There is an exception for the transfer of evanescent waves in the far field. Pendry theoretically predicted that a lossless slab made with left-handed material functions as a perfect lens when both $\varepsilon = -1$ and $\mu = -1$ are satisfied.[6] In general, a metamaterial (MM) slab, with both negative permittivity ε and permeability μ, not only supports negative refraction but also has the ability to restore evanescent waves in the far field and image beyond the diffraction limit.[7–9] A pioneering experiment verified subwavelength imaging in a two-dimensional transmission-line system where the loaded series capacitors and shunt inductors provide the left-handed electromagnetic response.[10] Appropriate and delicate design of subwavelength-sized metallic resonant structures is required to ensure simultaneously negative ε and μ in a certain frequency range. However, this is not easy to accomplish, especially for three-dimensional (3D) left-handed MMs in which spatial dispersion is usually very strong.

Subwavelength imaging can also be achieved with single-negative-index MMs in which the effective permittivity or permeability is negative and the other is positive. The electric and magnetic field components in a single-negative-index MM are largely decoupled when looking into the very near-field regime under the electrostatic limit.[11] This feature presents a feasible way for subwavelength imaging. For instance, a silver superlens with negative permittivity gives rise to a $\lambda/6$ spatial resolution in imaging for an object in the near field by "amplifying" electric fields.[12] Similarly, a *magnetic* image with a resolution down to $\lambda/64$ is generated by a μ-negative slab constructed with a "Swiss roll."[11] Such a superlens effect in single-negative-index MMs primarily relies on the excitation of surface modes and generates image spots bound to the lens-air interface.

Among various types of MMs for negative refraction, fishnet structures have attracted tremendous attention due to their high figure of merit and superior performance in optical frequencies.[13–18] Moreover, the planar structures of fishnet MMs are favorable for fabrication and present a feasible route for realization of 3D MMs. For conventional ways to utilize fishnet MMs, the electromagnetic waves are incident on surface of the metallic layer perforated with hole arrays, and the dimension of the metallic holes determines the maximum operational wavelength, i.e., the cutoff frequency of fishnet MMs. There is an alternative scheme that can drive fishnet MMs below the cutoff frequency. A theoretical study predicted all-angle negative refraction at frequencies below the cutoff frequency, provided that the incident light impinges on the sidewall interface of the fishnet stack.[19] The negative coupling among the propagating waves guided in the slab waveguides which are sandwiched by metallic layers generates a hyperbolic dispersion.[20–24] This type of hyperbolic dispersion leads to all-angle negative refraction in our fishnet MM. Recently, the same scheme was also proposed for acoustic waves.[25] However, there is no experimental report on such subwavelength-imaging functionality for fishnet MMs.

In this paper, we theoretically and experimentally demonstrate subwavelength imaging with 3D fishnet MMs at the microwave regime. The finite-difference time-domain (FDTD) simulations show that the image spot of a magnetic dipole source is $\lambda/3$ in size, exhibiting a superresolution feature. Further the local field measurement proves that the image of a ring antenna with a diameter of $\lambda/6$ has a full width at half maximum (FWHM) of $\lambda/2$, which agrees well with the theoretical predictions while taking into account the size effect of the source. Additional calculations indicate that the subwavelength imaging is valid in a broad frequency range.

II. ALL-ANGLE NEGATIVE REFRACTION

Figure 1(a) shows the schematic of our fishnet model and incident waves. The metal/dielectric layers, lying in the xy plane, are stacked alternately along the z direction.

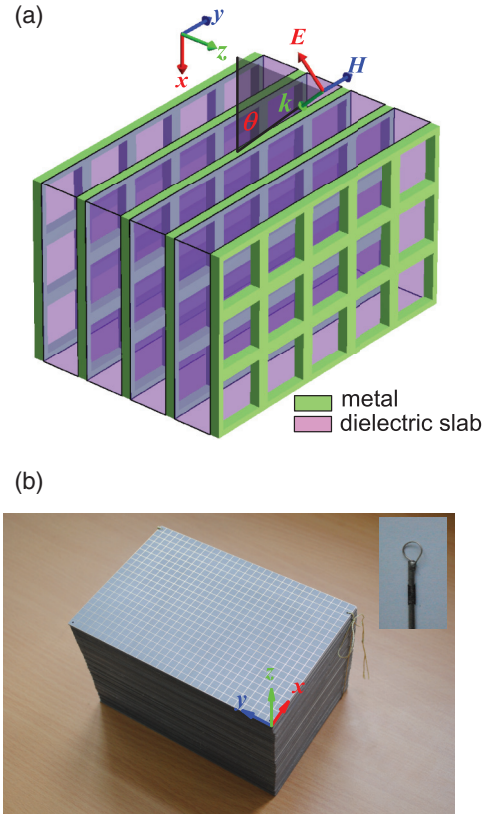

FIG. 1. (Color online) (a) Schematic of our fishnet model and the incidence configuration. (b) Photos of our fishnet sample and ring antenna (inset).

Each metallic layer, with a thickness of $t = 0.035$ mm, is perforated with hole arrays in a square lattice. The lattice period is $p_x = p_y = 6$ mm, and the size of the square holes is $a = 5.8$ mm. The allowed waveguide modes in a metallic hole have a cutoff frequency at $f_c = \frac{c_0}{2a} \approx 25.8$ GHz, where c_0 is the light velocity in vacuum. The dielectric layer has a thickness of $d = 1.575$ mm and a permittivity of $\varepsilon_r = 2.65$, which gives rise to a period of $p_z = d + t = 1.61$ mm in the z direction. The incident waves, propagating inside the xz plane with an incident angle of θ about the x axis, are transverse-magnetic (TM) polarized with magnetic field H along the y direction. At frequencies far below f_c, a single layer of holey metal can be homogenized to a Drude-type medium with a plasma frequency determined by f_c.[26] Also the stacked fishnet MM can be regarded as a spoof plasmonic waveguide array.[27–29] The layered metal-insulator-metal configuration of the fishnet MM forms waveguide channels in the xy plane, which only allow the quasi-TEM modes to propagate in the insulator layers. These modes, with electric field E along the z axis, can be well described with coupled-wave theory.[30,31] The holey metallic layers enable energy exchange among the adjacent waveguides, leading to a negative coupling coefficient and hyperbolic dispersion.[19,27] We perform the modal expansion method (MEM)[32–35] to calculate the dispersion of the fishnet system under TM polarization. The blue lines in Fig. 2 present the equifrequency surface (EFS) at 10 GHz, while the red circular line denotes the corresponding EFS in vacuum. It is noted that, when k_z

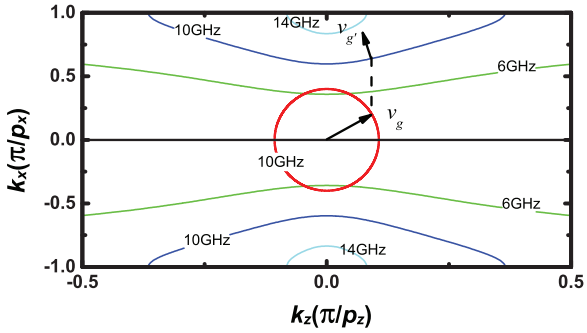

FIG. 2. (Color online) Equifrequency surface (EFS) in the fishnet MM at 10 GHz (blue line), 6 GHz (green line), and 14 GHz (cyan line) and the EFS in vacuum at 10 GHz (red circular line).

is relatively small, the effective electromagnetic parameters of fishnet MM form a hyperbolic dispersion of an anisotropic medium,

$$\frac{k_x^2}{\varepsilon_z \mu_y} + \frac{k_z^2}{\varepsilon_x \mu_y} = \frac{\omega^2}{c_0^2},$$

where $\varepsilon_z > 0$ and $\varepsilon_x < 0$ are the z and x components of the permittivity tensor, respectively, and $\mu_y > 0$ is the y component of the permeability tensor. k_x and k_z are the x and z components of the wave vector in the anisotropic medium, respectively, and ω is the angular frequency. Black arrows in Fig. 2 schematically denote the direction of group velocity (energy flow) $\vec{v}_g = \nabla_{\vec{k}}\omega(\vec{k})$, which is normal to the EFS and along the direction towards higher frequency. It can be seen from Fig. 2 that the transverse wave vector of the incident waves will be much smaller than π/p_z. In this regime, the EFS remains in a hyperbolic line shape, and negative refraction always occurs in the fishnet structure for all incident angles.

To verify the theoretical predictions of all-angle negative refraction, we perform FDTD numerical simulations by assuming a Gaussian beam incident on the sidewall interface of our fishnet MM from air. In the simulations, the finite-sized fishnet model has 60 periods in the x direction and 500 periods in the z direction. Periodic boundary conditions are applied along the y direction. The technique of perfect matched layers (PMLs) is applied at the x and z boundaries to absorb reflected waves. A one-way Gaussian beam source, which is TM polarized with magnetic field along the y direction ($H_x, H_z = 0$) at frequency $f = 10$ GHz, is positioned in the yz plane and 100 mm away from the top interface. The beam waist is 120 mm. Figure 3 presents the spatial distribution of the real part of the magnetic field component H_y in the xz plane with respect to different incident angles $\theta = 10°, 20°, 40°, 50°$. With the color recording the intensity of the local field at a point, Fig. 3 explicitly illustrates the path of the light beam propagating inside the fishnet system and in free space. We see from Fig. 3 that the negative refraction occurs at all the considered incident angles. Further the fishnet system is essentially transparent due to the mode matching between free-space photons and the quasi-TEM modes that propagate in the spoof plasmonic waveguide arrays, contributing to the high efficiency of the device.

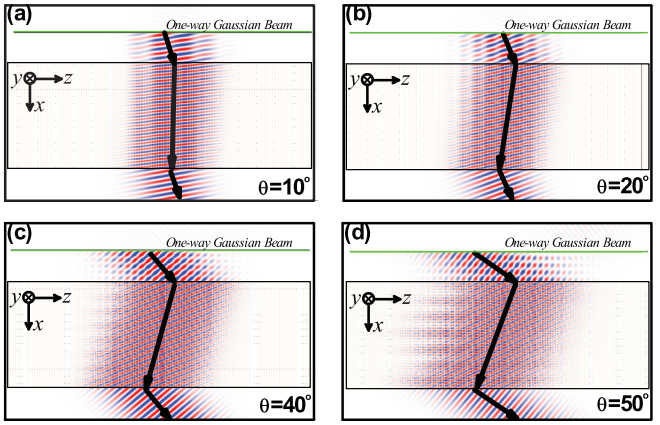

FIG. 3. (Color online) Negative refraction calculated at 10 GHz for different incident angles (a)–(d) $\theta = 10°,20°,40°,50°$ of a Gaussian beam. The real part of the magnetic field H_y in the snapshot is marked by red/blue for positive/negative values. The black arrows denote the propagating direction (Poynting vector) of the light beam.

III. EXPERIMENTS OF SUBWAVELENGTH IMAGING

The fishnet MMs provide local and global geometric parameters for tuning the hyperbolic dispersion and impedance matching at the air-fishnet interface and have been recognized as the most promising candidates for negative refraction in the visible and other frequency regimes. The scheme utilizing the sidewall of a stacked fishnet system as the incident interface presents a practical flat-lens solution for subwavelength imaging. Here we fabricate a 3D fishnet MM by printed-circuit-board (PCB) fabrication technology and experimentally investigate the subwavelength imaging with the local field measurement. A photo of the sample is shown in Fig. 1(b). The fishnet sample is a stack of 80 PCB slabs. The dielectric substrate in a PCB slab has a dielectric constant of $\varepsilon_r = 2.65$ and a thickness of $d = 1.575$ mm. The lateral size of a PCB slab is 120 mm in the x direction and 180 mm in the y direction. We use two small ring antennas made with coaxial cable to measure the magnetic field at a local point, as shown in the inset of Fig. 1(b). The source antenna is placed about 10 mm away from the sidewall of the fishnet MM. The probe antenna, on the other side of the sample, is arranged on a movable table electrically driven by a computer to scan the magnetic local field. An Agilent 8722ES network analyzer is used to measure the complex transmission coefficient $\tilde{S}_{21}$. By scanning the probe at 1-mm intervals with the two-dimensional table, we map the magnetic local field intensity $|\tilde{S}_{21}|^2$ as a function of probe position (x,z) at a frequency of 10 GHz, as shown in Fig. 4. It is noted that an image spot is measured at a distance of 19 mm away from the outgoing interface of the fishnet sample. Figure 5(a) plots the intensity of magnetic fields at 10 GHz as a function of z along the line at $x = 19$ mm in the image plane. We can see that the FWHM is 15 mm (equal to $\lambda/2$) at critical subdiffraction resolution. Numerical simulations show that the FWHM of an ideal point source is about 10 mm ($\lambda/3$), as shown in Fig. 5(b). The diameter of the ring antenna is 5 mm. As the coaxial cable has a dimension of about 2 mm, an antenna with a diameter smaller than 5 mm cannot guarantee the desired linear polarization (TM polarization) in our experiments. Considering that the antennas are not ideal

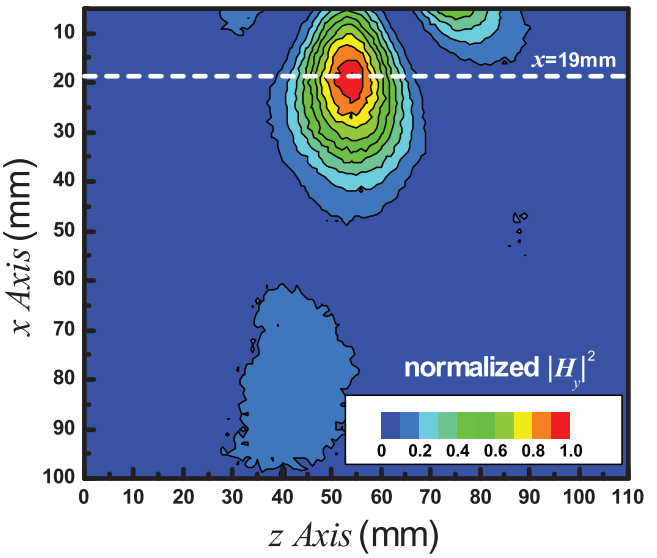

FIG. 4. (Color online) Measured image at 10 GHz of a small ring antenna as an object which is about 10 mm away from the fishnet flat lens. The white dashed line denotes the x coordinate of the image spot, which is 19 mm away from the lens-air interface.

point sources, we conclude that the measured image size of $\lambda/2$ is within the range of subdiffraction resolution. By comparing the arbitrary values of magnetic fields at the image plane

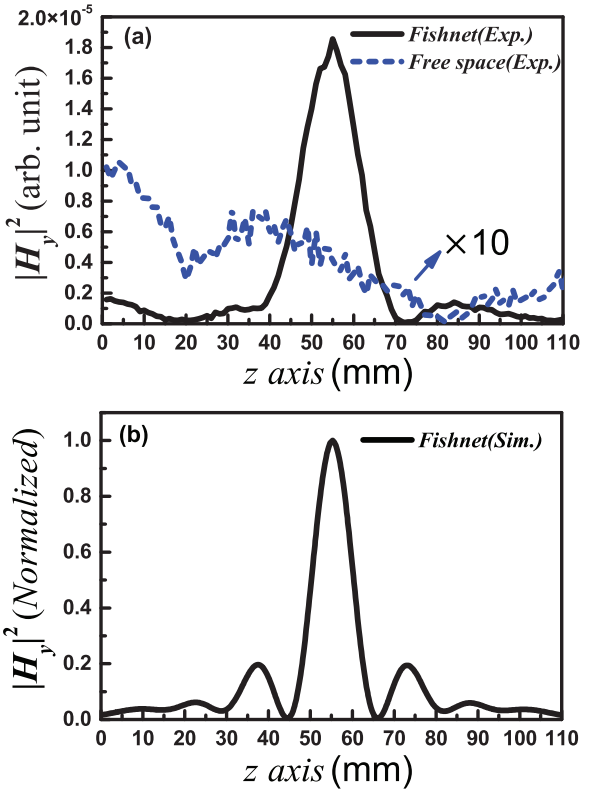

FIG. 5. (Color online) Magnetic field intensity $|H_y|^2$ at a line of $x = 19$ mm as a function of the z coordinates. (a) Measured results with/without a fishnet flat lens (solid/dashed line) for a ring antenna with a diameter of 5 mm as the object and (b) calculated results for an ideal magnetic dipole source as the object.

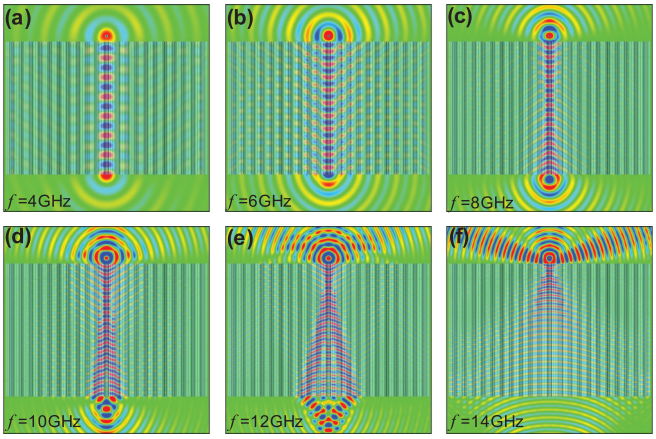

FIG. 6. (Color online) (a)–(f) Calculated imaging of a point source through the fishnet lens at $f = 4$, 6, 8, 10, 12, and 14 GHz, respectively. The distance between the point source and the lens is fixed at 15 mm.

with and without a fishnet MM sample [see the solid and dashed lines in Fig. 5(a)], we find that the former is about 50 times larger than the latter at the center of the image spot, implying a high efficiency in imaging.

The all-angle negative refraction of the fishnet MMs comes from the light coupling of quasi-TEM modes propagating in the spoof plasmonic waveguide arrays where the coupling coefficient remains negative in a wide frequency range starting from zero frequency. Consequently, the subwavelength imaging also exhibits a broadband property. Nevertheless, the coupling between the adjacent waveguides becomes weaker and weaker at lower frequencies, and a large enough thickness along the x direction of the fishnet flat lens is required for imaging. We perform FDTD simulations to verify the broadband subwavelength imaging. The model of a fishnet MM has 60 periods along the x direction. Figure 6 shows the calculated magnetic field distributions H_y at different frequencies $f = 4$, 6, 8, 10, 12, and 14 GHz. In the FDTD simulations, the magnetic point source is located 15 mm away from the air-fishnet interface at the incident side. We can see that a real image spot appears at frequencies f =8, 10, 12, and 14 GHz, as shown in Figs. 6(c)–6(f), respectively. At lower frequencies $f = 4$ and 6 GHz [Figs. 6(a) and 6(b)], the collimation effect, as a weaker version of negative refraction, is dominant, and no real image is observed as the model is too thin. Additional calculations (not shown) indicate that a real image can be readily obtained below 6 GHz by adopting a larger model with enough thickness, provided that the object is at the proximity of the air-fishnet interface.

IV. CONCLUSIONS

In summary, we have theoretically and experimentally investigated subwavelength imaging of a flat lens which utilizes the sidewall interface of stacked fishnet MMs. By adopting a ring antenna with a small electrical size as an object, we observed a high-quality image with a size no more than half of the operational wavelength. Measured results agree well with the FDTD simulations. Additional calculations verified that negative refraction and subwavelength imaging can be readily obtained in a broad frequency range, even at much lower frequencies. The findings are helpful for understanding the underlying physics of the electromagnetic response of fishnet MMs, which may have great potential for devices in microwave, terahertz, and even optical regimes.

ACKNOWLEDGMENTS

This work was supported by the 863 Major Program (Grant No. 2012AA03A706), NSFC (Grants No. 10974144, No. 11174221, No. 11204218, and No. 61205041), CNKBRSF (Grant No. 2011CB922001), the Fundamental Research Funds for the Central Universities, SHEDF (Grant No. 06SG24), and the China Postdoctoral Science Foundation (Grants No. 2011M500810, No. 2012T50433, and No. 2012M520922).

*hqlee@tongji.edu.cn

[1] M. Born and E. Wolf, *Principles of Optics: Electromagnetic Theory of Propagation, Interference and Diffraction of Light* (Pergamon, Oxford, 1980).
[2] T. Brunet, J. L. Thomas, and R. Marchiano, Phys. Rev. Lett. **105**, 034301 (2010).
[3] Z. Y. Wang, Y. Luo, T. Jiang, Z. Wang, J. T. Huangfu, and L. X. Ran, Phys. Rev. Lett. **106**, 047402 (2011).
[4] E. T. F. Rogers, J. Lindberg, T. Roy, S. Savo, J. E. Chad, M. R. Dennis, and N. I. Zheludev, Nat. Mater. **11**, 432 (2012).
[5] R. Sapienza, T. Coenen, J. Renger, M. Kuttge, N. F. van Hulst, and A. Polman, Nat. Mater. **11**, 781 (2012).
[6] J. B. Pendry, Phys. Rev. Lett. **85**, 3966 (2000).
[7] D. R. Smith, J. B. Pendry, and M. C. K. Wiltshire, Science **305**, 788 (2004).
[8] N. Engheta and R. W. Ziolkowski, *Metamaterials: Physics and Engineering Explorations* (Wiley-IEEE Press, New York, 2006).
[9] W. Cai and V. Shalaev, *Optical Metamaterials: Fundamentals and Applications* (Springer, New York, 2009).
[10] A. Grbic and G. V. Eleftheriades, Phys. Rev. Lett. **92**, 117403 (2004).
[11] M. Wiltshire, J. Pendry, and J. Hajnal, J. Phys. Condens. Matter **18**, L315 (2006).
[12] N. Fang, H. Lee, C. Sun, and X. Zhang, Science **308**, 534 (2005).
[13] G. Dolling, C. Enkrich, M. Wegener, C. M. Soukoulis, and S. Linden, Science **312**, 892 (2006).
[14] C. Garcia-Meca, J. Hurtado, J. Marti, A. Martinez, W. Dickson, and A. V. Zayats, Phys. Rev. Lett. **106**, 067402 (2011).
[15] J. M. Hamm, S. Wuestner, K. L. Tsakmakidis, and O. Hess, Phys. Rev. Lett. **107**, 167405 (2011).
[16] J. Valentine, S. Zhang, T. Zentgraf, E. Ulin-Avila, D. A. Genov, G. Bartal, and X. Zhang, Nature (London) **455**, 376 (2008).
[17] S. Wuestner, A. Pusch, K. L. Tsakmakidis, J. M. Hamm, and O. Hess, Phys. Rev. Lett. **105**, 127401 (2010).
[18] J. Yang, C. Sauvan, H. T. Liu, and P. Lalanne, Phys. Rev. Lett. **107**, 043903 (2011).
[19] Z. Y. Wei, Y. Cao, J. Han, C. Wu, Y. C. Fan, and H. Q. Li, Appl. Phys. Lett. **97**, 141901 (2010).

[20]J. Yao, Z. W. Liu, Y. M. Liu, Y. Wang, C. Sun, G. Bartal, A. M. Stacy, and X. Zhang, Science **321**, 930 (2008).
[21]L. Menon, W. T. Lu, A. L. Friedman, S. P. Bennett, D. Heiman, and S. Sridhar, Appl. Phys. Lett. **93**, 123117 (2008).
[22]W. Li, Z. Liu, X. G. Zhang, and X. Y. Jiang, Appl. Phys. Lett. **100**, 161108 (2012).
[23]Y. M. Liu, G. Bartal, and X. Zhang, Opt. Express **16**, 15439 (2008).
[24]A. Fang, T. Koschny, and C. M. Soukoulis, Phys. Rev. B **79**, 245127 (2009).
[25]J. Christensen and F. J. G. de Abajo, Phys. Rev. Lett. **108**, 124301 (2012).
[26]J. B. Pendry, L. Martin-Moreno, and F. J. Garcia-Vidal, Science **305**, 847 (2004).
[27]X. Fan, G. P. Wang, J. C. W. Lee, and C. T. Chan, Phys. Rev. Lett. **97**, 073901 (2006).
[28]L. Verslegers, P. B. Catrysse, Z. F. Yu, and S. H. Fan, Phys. Rev. Lett. **103**, 033902 (2009).
[29]E. Verhagen, R. de Waele, L. Kuipers, and A. Polman, Phys. Rev. Lett. **105**, 223901 (2010).
[30]H. Haus and L. Molter-Orr, IEEE J. Quantum Electron. **19**, 840 (1983).
[31]T. Pertsch, T. Zentgraf, U. Peschel, A. Brauer, and F. Lederer, Phys. Rev. Lett. **88**, 093901 (2002).
[32]P. Sheng, R. S. Stepleman, and P. N. Sanda, Phys. Rev. B **26**, 2907 (1982).
[33]P. Lalanne, J. P. Hugonin, S. Astilean, M. Palamaru, and K. D. Moller, J. Opt. A **2**, 48 (2000).
[34]Y. Cao, Z. Y. Wei, C. Wu, H. Q. Li, H. Chen, and K. Cai, Opt. Express **20**, 25520 (2012).
[35]Z. Y. Wei, Y. Cao, X. P. Su, Z. J. Gong, Y. Long, and H. Q. Li, Opt. Express **21**, 10739 (2013).